Supporting Information

0D Hybrid Lead-free Halide with Near-unity Photoluminescence Quantum Yield toward Multifunctional Optoelectronic Applications

Dong-Yang Li,† Huai-Yuan Kang,† Yu-Hang, Liu, Jie Zhang, Cheng-Yang Yue, Dongpeng Yan,* and Xiao-Wu Lei*

Dong-Yang Li, Prof. Cheng-Yang Yue, Prof. Xiao-Wu Lei
School of Chemistry, Chemical Engineer and Materials, Jining University, Qufu, Shandong, 273155, P. R. China
E-mail: xwlei_jnu@163.com

Prof. Dongpeng Yan
Beijing Key Laboratory of Energy Conversion and Storage Materials, College of Chemistry, and Key Laboratory of Radiopharmaceuticals, Ministry of Education, Beijing Normal University, Beijing 100875, P. R. China
E-mail: yandp@bnu.edu.cn

Dong-Yang Li, Yu-Hang Liu, Jie Zhang
School of Chemistry and Chemical Engineering, Qufu Normal University, Qufu, Shandong, 273165, P. R. China

† Dong-Yang Li and Huai-Yuan Kang contributed equally to this work.

Experimental Section

Materials: The chemical materials were commercially purchased from Aladdin chemical company and directly used without any further purification. $InCl_3 \cdot 4H_2O$ (99.99%), $SbCl_3$ (99.99%), 3,3′-iminobis (N,N-dimethylpropylamine) (Im-BDMPA, $C_{10}H_{25}N_3$, 97%), hydrochloric acid (HCl, 37%), ethanol (EtOH, 99%), isobutanol (99%), acetonitrile (99%), acetone (99%), Epoxy resin ab adhesive, Sylgard 184 elastomer kit, Dow corning and polytetrafluoroethylene mode.

Synthesis of (Im-BDMPA)$InCl_6 \cdot H_2O$ and (Im-BDMPA)$In_{0.78}Sb_{0.22}Cl_6 \cdot H_2O$ crystals: 0.2932 g $InCl_3 \cdot 4H_2O$ and 0.1873 g Im-BDMPA were added to the mixed solution of HCl (1 mL), isobutanol (3 mL) and acetonitrile (2 mL) with continuously heating and stirring to dissolve. Then the solution was transferred into a 15 mL glass vial and heated at 80 °C for 5 days. After cooling down to 25 ℃, the colorless plate-like crystals were collected by filtration and determined as (Im-BDMPA)$InCl_6 \cdot H_2O$ ($C_{10}H_{27}N_3OInCl_6$) by single-crystal XRD. The crystals were washed with methanol three times and stored in a sealed bottle (yield of 90% based on $InCl_3$). The simulated elemental contents of $C_{10}H_{27}N_3OInCl_6$ were calculated to be 22.53% and 7.88% for C and N elements, respectively, which match with the experimental results (C = 22.55%; N = 7.90%). The colorless crystals of (Im-BDMPA)$In_{0.78}Sb_{0.22}Cl_6 \cdot H_2O$ were prepared via the same reaction condition with the addition of $SbCl_3$ (0.1145 g).

Synthesis of (Im-BDMPA)Cl_3: Briefly, Im-BDMPA was firstly added into HCl to form clear solution and then condensed via rotary evaporation to form white powder. The obtained powder was washed with ethanol for several times and finally collected after drying in vacuum oven.

Solid phase synthesis of (Im-BDMPA)$In_{0.78}Sb_{0.22}Cl_6 \cdot H_2O$: Mixture of $SbCl_3$ (0.1145 g), $InCl_3 \cdot 4H_2O$ (0.2932 g) and (Im-BDMPA)Cl_3 (0.187 g) was ground together using a mortar and

pestle for about 15 minutes. A white microscale powder of (Im-BDMPA)$In_{0.78}Sb_{0.22}Cl_6 \cdot H_2O$ was obtained and used for further studies.

Synthesis of (Im-BDMPA)$In_{0.78}Sb_{0.22}Cl_6 \cdot H_2O$ microparticles: (Im-BDMPA)$In_{0.78}Sb_{0.22}Cl_6 \cdot H_2O$ crystals were ground for 5 hours using an agate mortar and pestle. After that, the resulted powders were dispersed in ethanol solvent, which was then placed in a microwave digestion tank and heated in a microwave oven at 500 W for 20 h. Afterward, the suspension of (Im-BDMPA)$In_{0.78}Sb_{0.22}Cl_6 \cdot H_2O$ was separated by centrifugation to get the microparticles. Finally, the resulted microparticles were washed by ethanol and dried in a vacuum drier at 50 °C for 30 h.

Preparation of (Im-BDMPA)$In_{0.78}Sb_{0.22}Cl_6 \cdot H_2O$ flexible films: The flexible film was prepared by dissolving a silicone elastomer (Epoxy resin ab adhesive) and a cross-linker (Sylgard 184 elastomer kit, Dow Corning) in 10 mL acetone with stirring at room temperature for at 8 h to get a dispersed solution. Afterward, (Im-BDMPA)$In_{0.78}Sb_{0.22}Cl_6 \cdot H_2O$ microparticles were added into the mixture and stirred for 15 hours. Then the solution was poured into a polytetrafluoroethylene mold, which was placed into a vacuum oven and dried at 50 °C overnight to evaporate the solvent.

Single crystal X-ray diffraction: The single crystal data of (Im-BDMPA)$InCl_6 \cdot H_2O$ was collected on the Bruker Apex II CCD diffractometer with Cu-*K*α radiation (λ = 1.3405) at room temperature. All the non-hydrogen atoms were refined with anisotropic thermal parameters, and hydrogen atoms of organic molecules were positioned geometrically and refined isotropically. Structural refinement parameters of compound (Im-BDMPA)$InCl_6 \cdot H_2O$ (CCDC number 2233592) is summarized in Table S5 and important bond parameters are listed in Table S6-S7.

Common characterizations: The powder X-ray diffraction (PXRD) analysis was performed on

Bruker D8 ADVANCE powder X-ray diffractometer equipped with copper $K\alpha$ radiation at a voltage of 40 kV. The solid state UV-Vis absorption optical spectrum was collected at PE Lambda 900 UV/Vis spectrophotometer at room temperature in wavelength range of 200-800 nm. The PL spectrum, PLQY measurement and time-resolved decay data were performed on an Edinbergh FLS980 fluorescence spectrometer. The corresponding Commission Internationale Eclairage (CIE) chromaticity coordinates are calculated based on emission spectrum. The thermogravimetric analysis (TGA) was carried out on a Mettler TGA/SDTA 851 thermal analyzer in the temperature range of 30-800°C under the constant protection of N_2 atmosphere flow. The Raman measurement was performed on powder sample in the range of 50-4000 cm^{-1} by using Horiba Scientific LabRam HR Evolution under 365 nm excitation wavelength. The contents of elements (C, N, H) were determined by elemental quantitative analysis (EA) on a Elemantar: Vario EL cube. Elemental mapping was conducted on a scanning electron microscope (SEM, Zeiss Merlin Compact). The X-ray photoelectron spectroscopy (XPS) spectra were tested on the Escalab XI instrument. Inductively coupled plasma optical emission spectrometer measurement (ICP-OES) was performed on Agilent 5110. The X-ray photoelectron spectroscopy (XPS) spectrum was tested on the Escalab XI instrument, USA. SEM and DEX images were performed in Hitachi SU-8010 field emission scanning electron microscopy. By using the one-oscillator model and assuming a linear relationship between thermal expansion and temperature, the temperature-dependent PL emission energy evolution is fitted by the follow equation:

$$E_g(T) = E_0 + A_{TE}T + A_{EP}\left[\frac{2}{\exp\left(\frac{h_w}{K_B T}\right) - 1} + 1\right]$$

where E_0 is the unrenormalized band gap, $E_g(T = 0) = E_0 + A_{EP}$; A_{TE} and A_{EP} are the weight of TE

and EP interactions, respectively; h_ω is the average optical phonon energy; and k_B is Boltzmann's constant.

Fabrication of white LED lamp: The white LED lamp device was fabricated by coating the mixture of yellow phosphor (Im-BDMPA)$In_{0.78}Sb_{0.22}Cl_6 \cdot H_2O$ and commercial $BaMgAl_{10}O_{17}:Eu^{2+}$ blue phosphor on a 365 nm UV LED chip. These two phosphors were mixed with epoxy resin and stirred continuously for 15 min. Then the mixture was coated on the surface of the UV LED chip and cured for 30 min under vacuum conditions. The optical properties of the fabricated WLED was evaluated by a temperature-programmed LED optoelectronic analyzer with an integrating sphere (EVERFINE HAAS-2000).

X-Ray property characterization: The absorption coefficient (α) toward X-ray is mainly determined by the effective atomic number (Z_{eff}) as $\alpha \propto \rho Z_{eff}^4/E^3$, where ρ is mass density and E is the X-ray photon energy. The RL spectra were obtained on a FLS1000 fluorescence spectrometer equipped with an X-ray source (W-target, 12 W) at 50 kV. The X-ray imaging is acquired on a digital camera (CMOS), and edge spread function (ESF) is obtained from the slanted-edge profile of this X-ray image. The MTF profile is defined as follow:

$$MTF(v) = F(LSF(x)) = F(\frac{dESF(x)}{dx})$$

where v is the spatial frequency, and x is the position of the pixels.

Theoretical band calculation: The single crystal data of (Im-BDMPA)$In_{1-x}Sb_xCl_6 \cdot H_2O$ were directly used to calculate the electronic band structure in CASTEP software. The total energy was calculated with density functional theory (DFT) using Perdew-Burke-Ernzerhof (PBE) generalized gradient approximation. Hence, the C-$2s^22p^2$, N-$2s^22p^3$, H-$1s^1$, In-$5s^25p$, Sb-$5s^25p^3$ and Cl-$3s^23p^5$ orbital were adopted as valence electrons. The number of plane wave included in the basis sets was

determined by a cutoff energy of 320 eV and numerical integration of the Brillouin zone is performed using Monkhorst-Pack k-point sampling of 2×2×2. Other calculating parameters and convergence criteria were set by the default values of the CASTEP cod.

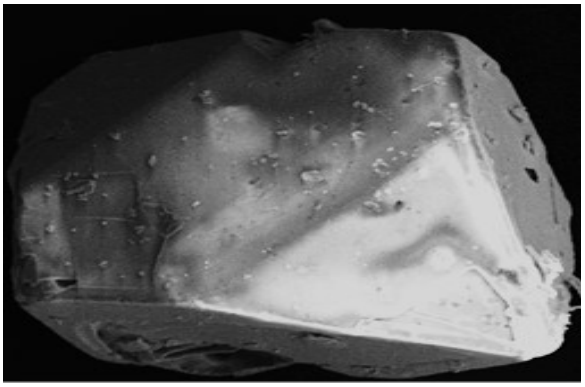

a

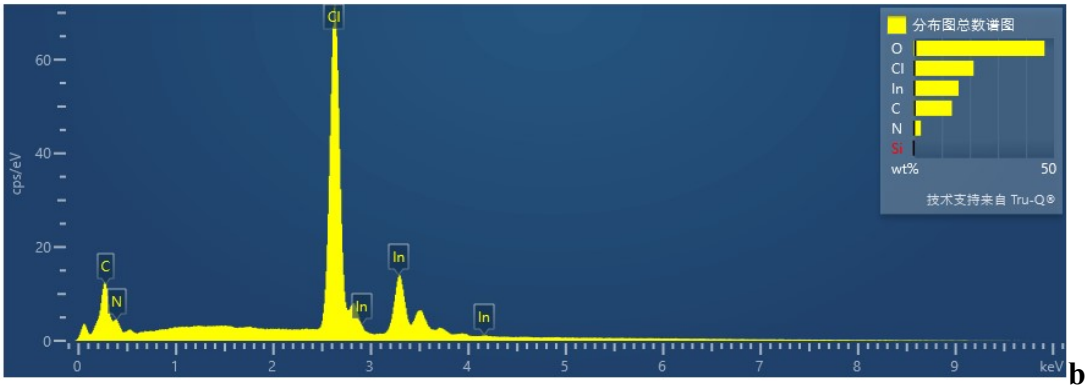

b

Fig. S1 a) SEM photo image and b) EDS result of (Im-BDMPA)$InCl_6 \cdot H_2O$ bulk crystal.

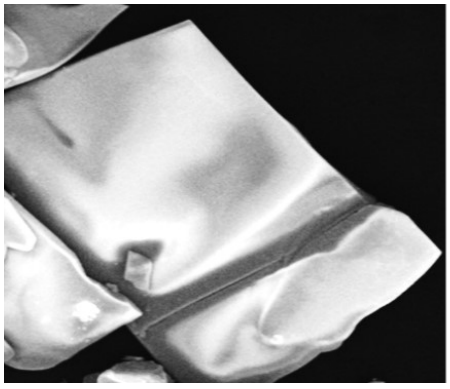

a

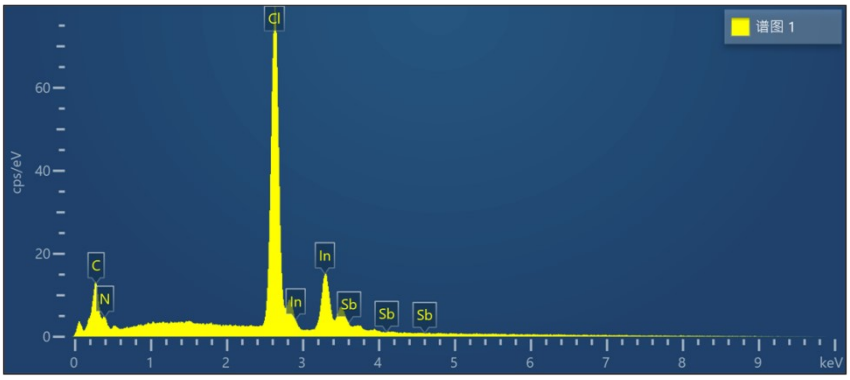

b

Fig. S2 a) SEM photo image and b) EDS result of (Im-BDMPA)$In_{0.78}Sb_{0.22}Cl_6 \cdot H_2O$ bulk crystal.

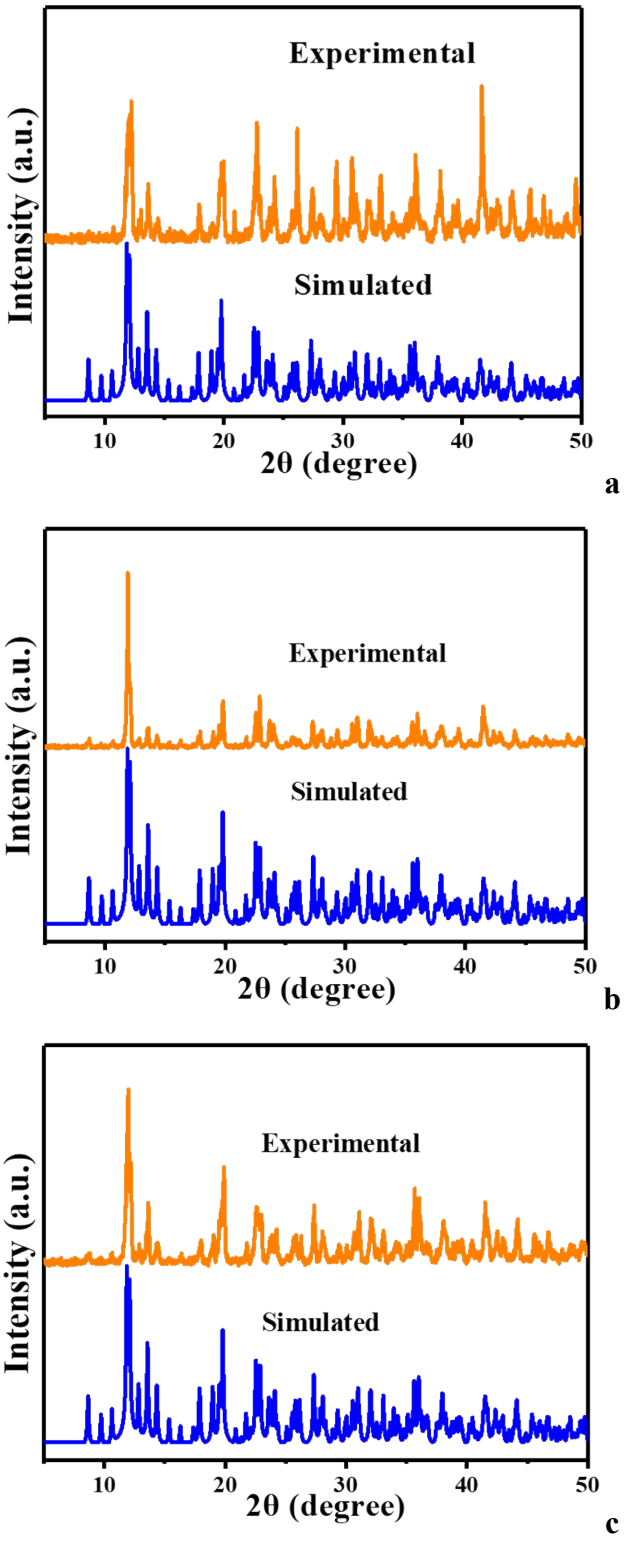

Fig. S3 The simulated and experimental PXRD patterns of (Im-BDMPA)$In_{0.78}Sb_{0.22}Cl_6 \cdot H_2O$ a) microparticle, b) deposited thin film and c) flexible device.

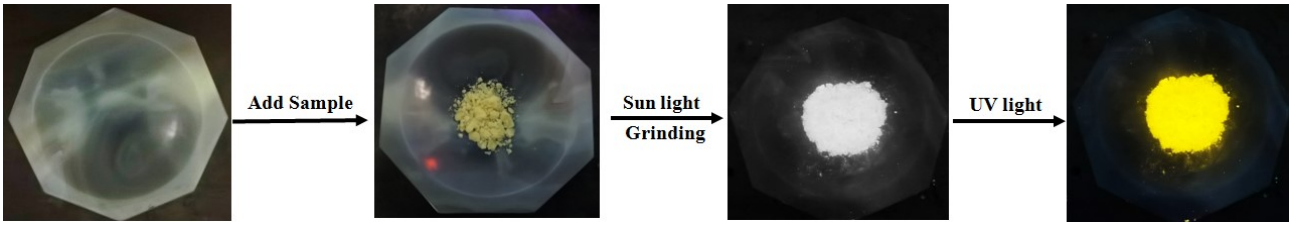

Fig. S4 Photo images of solid-phase preparation process of (Im-BDMPA)$In_{0.78}Sb_{0.22}Cl_6 \cdot H_2O$.

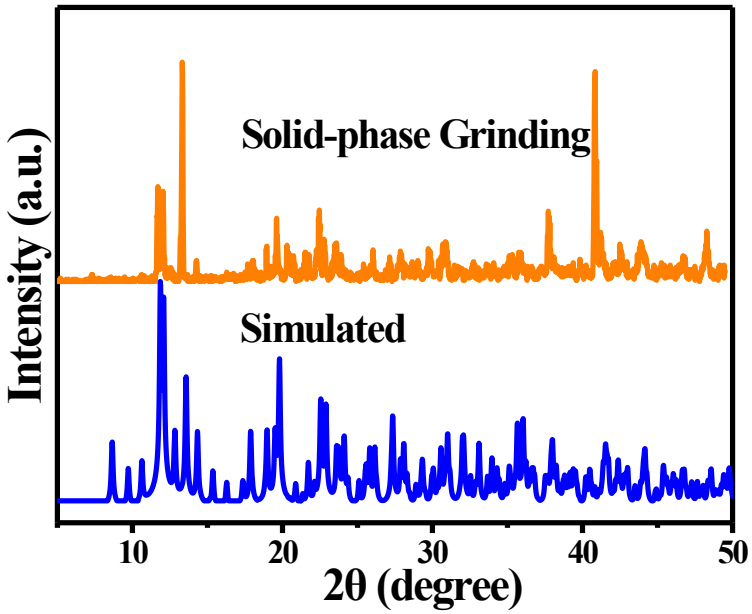

Fig. S5 The PXRD pattern of (Im-BDMPA)$In_{0.78}Sb_{0.22}Cl_6 \cdot H_2O$ prepared from solid-phase mechanical grinding method.

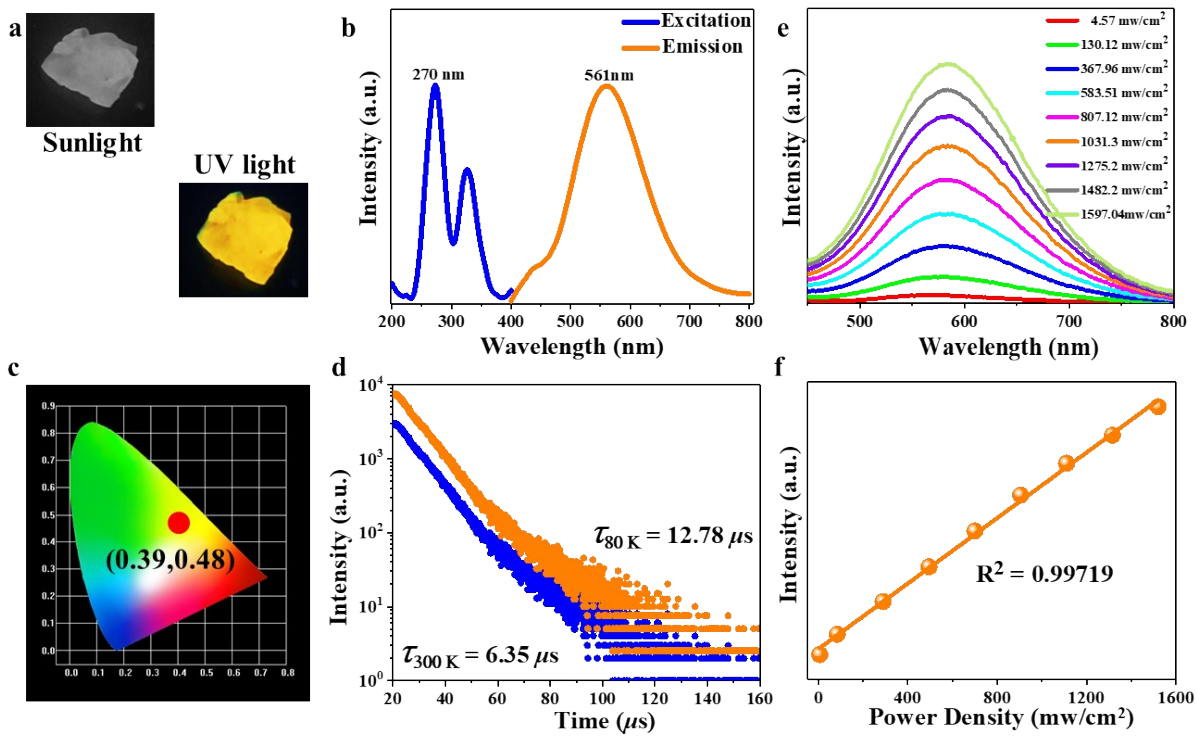

Fig. S6 Systematical PL characterizations of (Im-BDMPA)$InCl_6 \cdot H_2O$ bulk crystal: a) Photo images under sunlight and UV light; b) PLE and PL spectra; c) CIE coordinate; d) PL decay curves at 300 K and 80 K; e-f) Excitation power density dependent PL spectra.

Fig. S7 Photo images of deposited flexible device under sunlight (a) and 365 nm UV light (b).

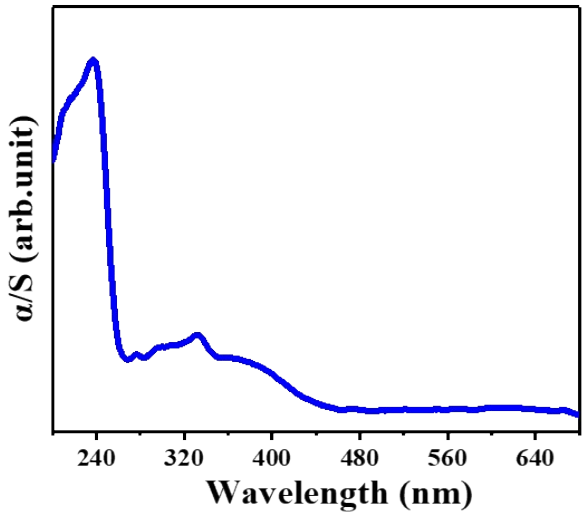

Fig. S8 The solid state UV-Vis absorption optical spectra of (Im-BDMPA)$InCl_6 \cdot H_2O$.

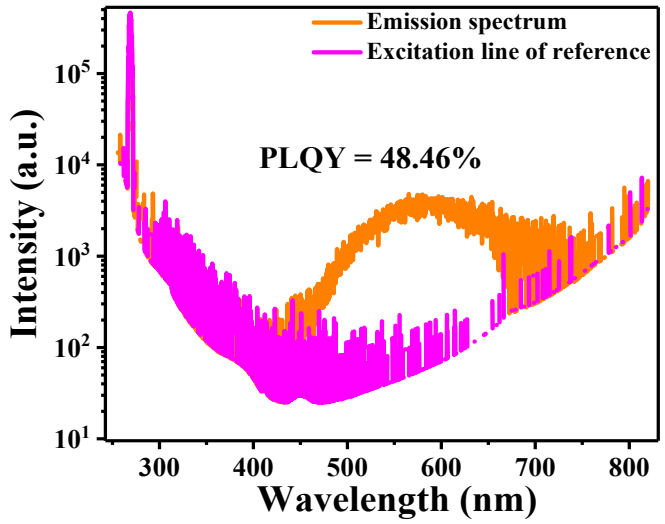

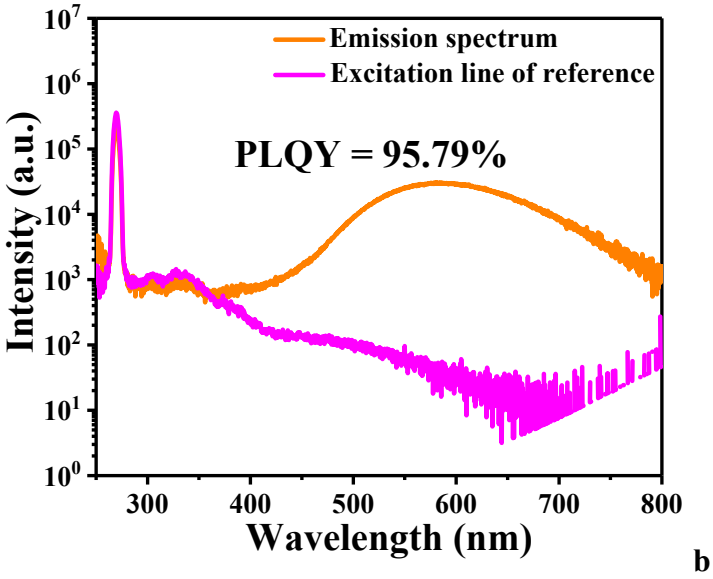

Fig. S9 PLQYs of a) (Im-BDMPA)$InCl_6 \cdot H_2O$ and b) (Im-BDMPA)$In_{0.78}Sb_{0.22}Cl_6 \cdot H_2O$ bulk crystals.

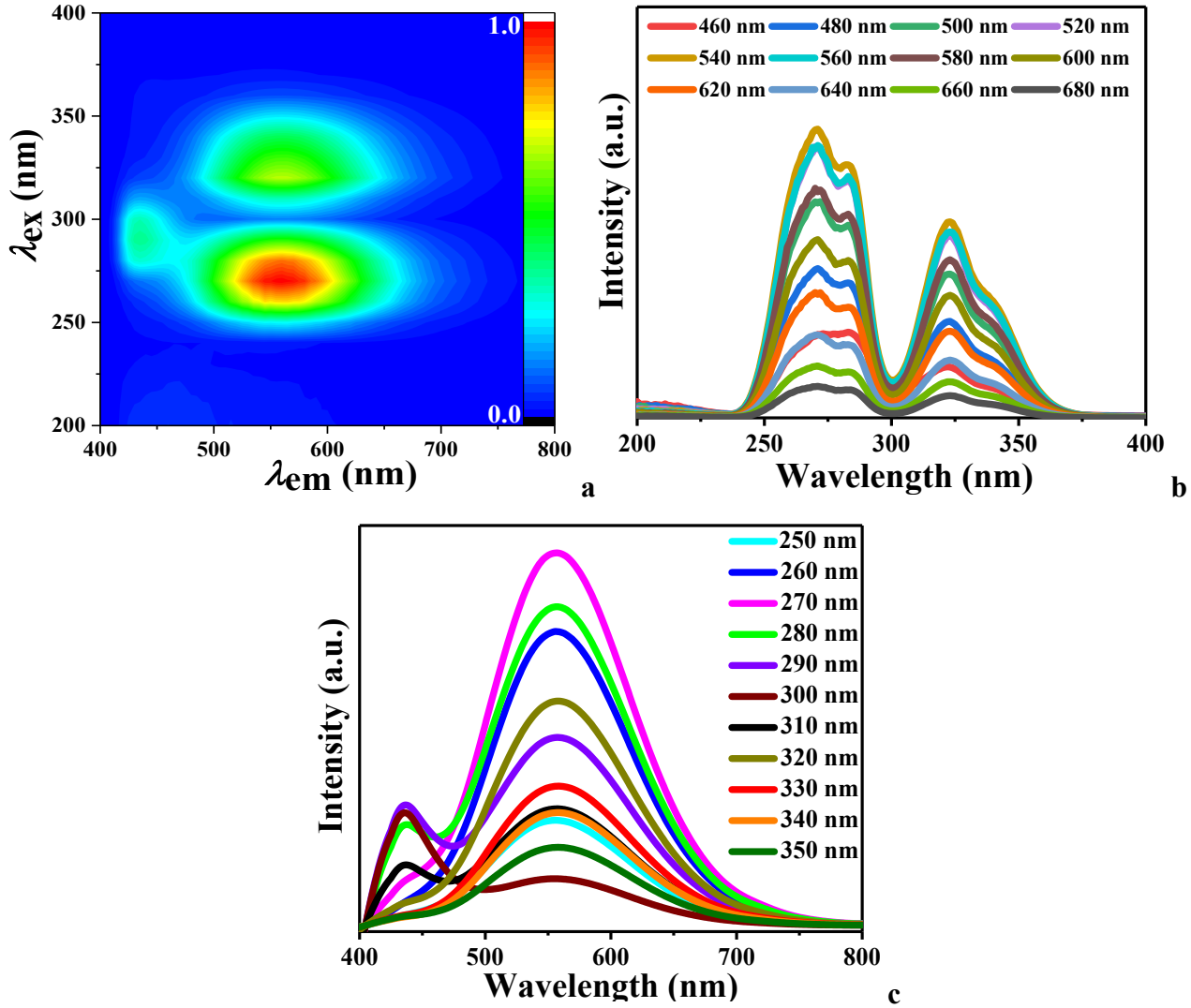

Fig. S10 a) 3D consecutive PL excitation and emission spectrum; b) Emission wavelength dependent excitation spectra; c) Excitation dependent emission spectra of (Im-BDMPA)$InCl_6 \cdot H_2O$ bulk crystal.

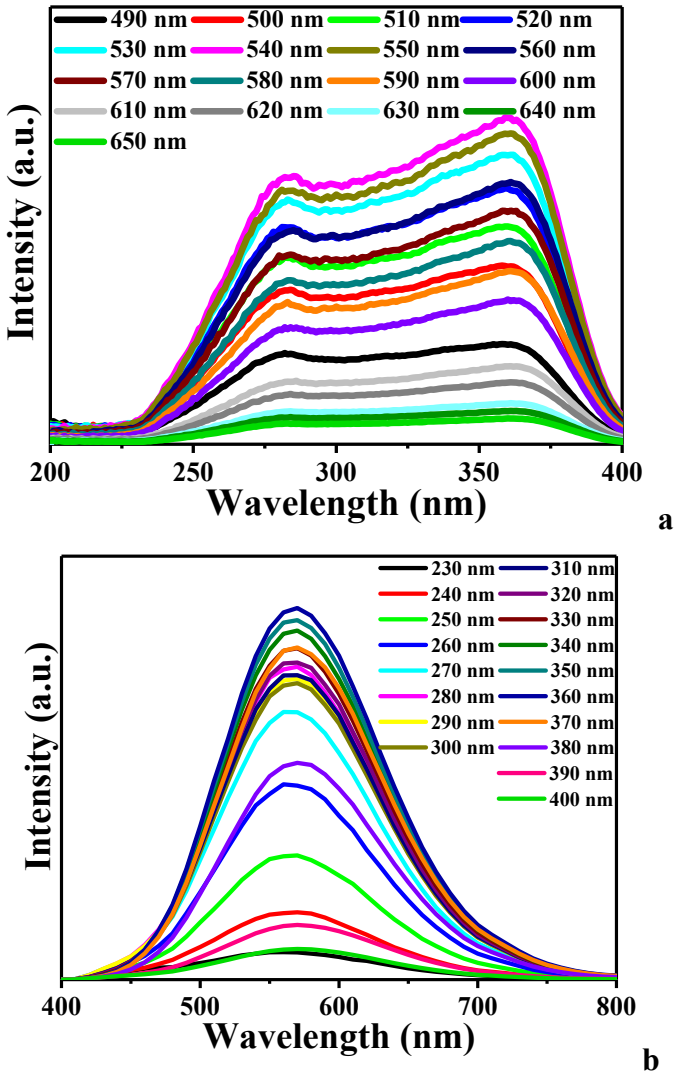

Fig. S11 a) Emission wavelength dependent excitation spectra; b) Excitation dependent emission spectra of (Im-BDMPA)$In_{0.78}Sb_{0.22}Cl_6 \cdot H_2O$ bulk crystal.

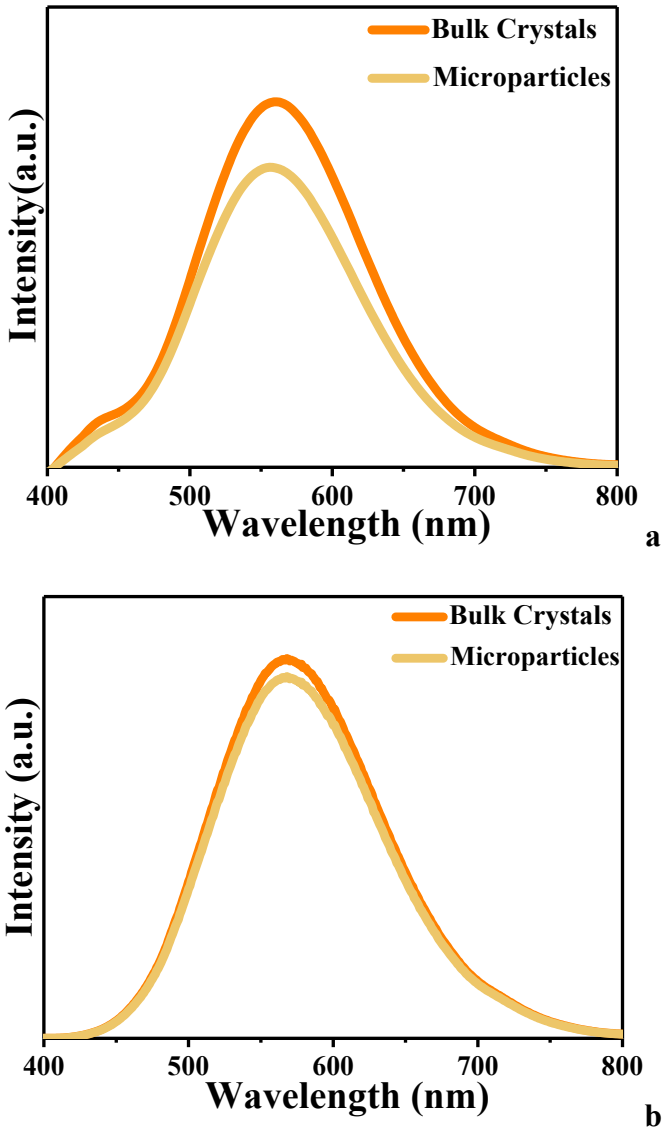

Fig. S12 Comparison of PL emission spectra of bulk crystal and microparticles for a) (Im-BDMPA)$InCl_6 \cdot H_2O$ and b) (Im-BDMPA)$In_{0.78}Sb_{0.22}Cl_6 \cdot H_2O$.

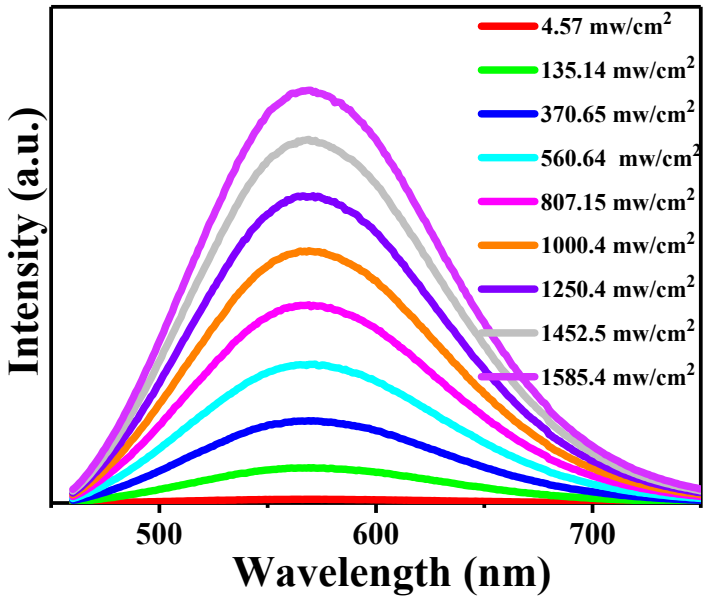

Fig. S13 Excitation power density dependent PL emission spectra of (Im-BDMPA)$In_{0.78}Sb_{0.22}Cl_6 \cdot H_2O$ bulk crystal.

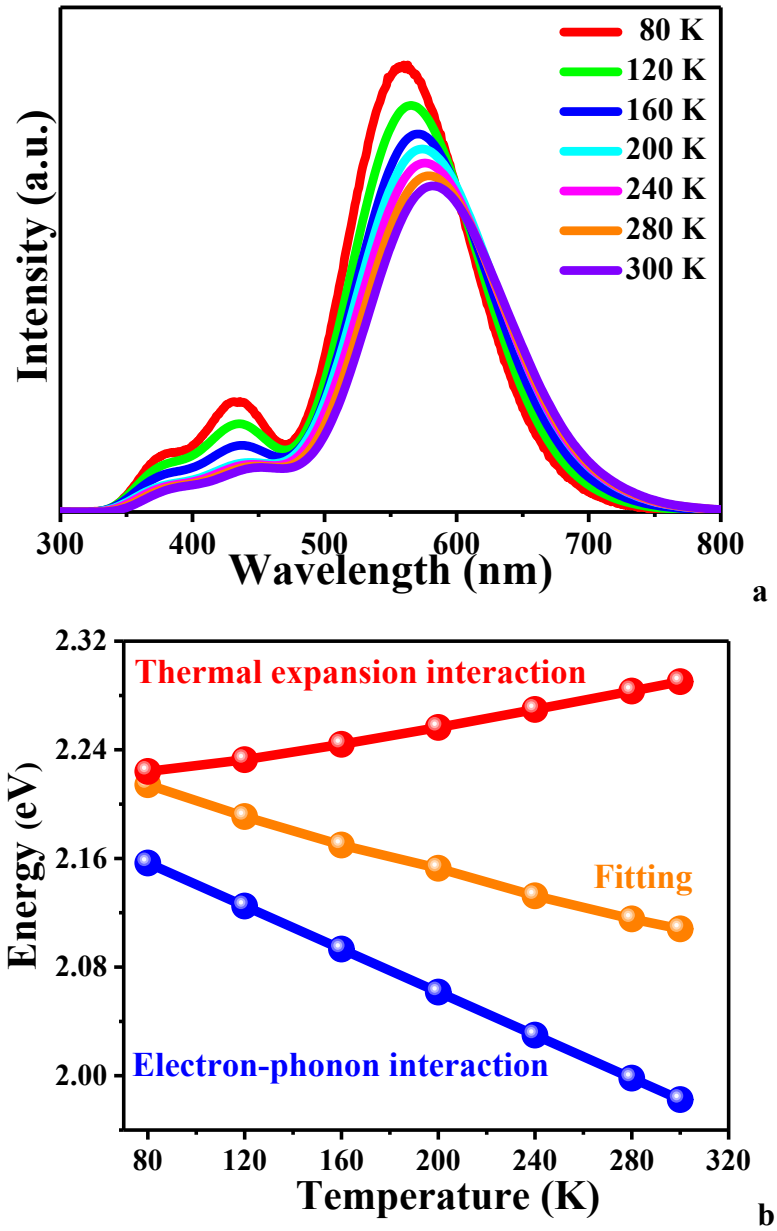

Fig. S14 a) Temperature dependent PL emission spectra from 300 K to 80 K; b) Temperature-dependent PL energy evolution of with the contribution of thermal expansion and electronic-phonon interactions of (Im-BDMPA)$In_{0.78}Sb_{0.22}Cl_6 \cdot H_2O$ bulk crystal.

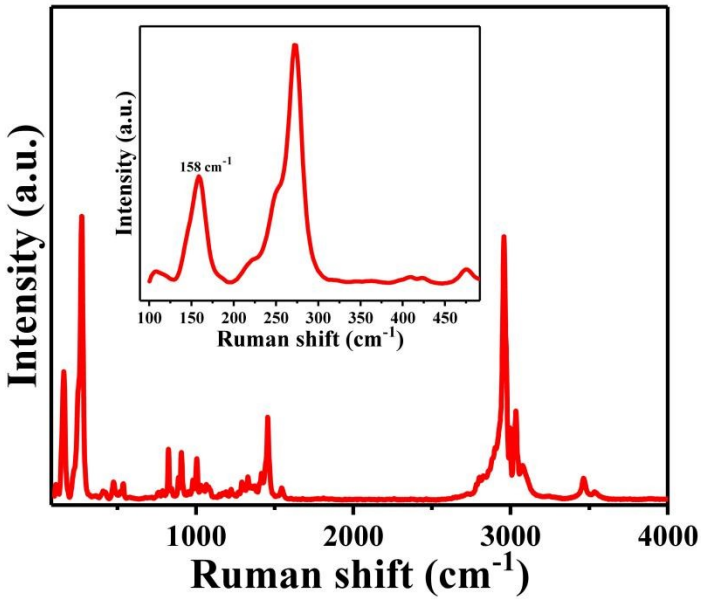

Fig. S15 Raman spectrum of (Im-BDMPA)$In_{0.78}Sb_{0.22}Cl_6 \cdot H_2O$ bulk crystal.

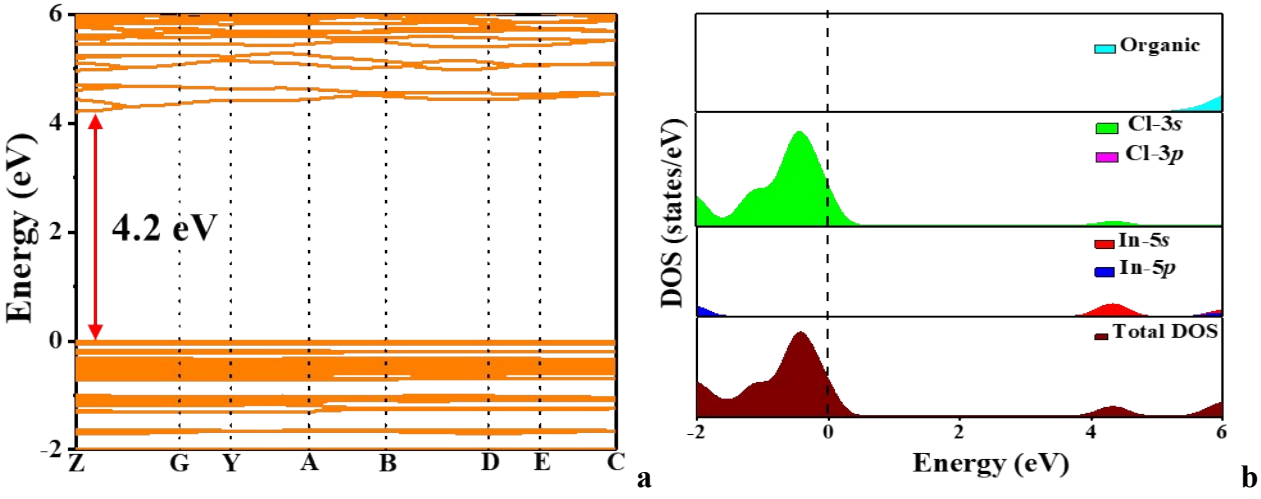

Fig. S16 Electronic band structure (a) and density of states (b) of (Im-BDMPA)$InCl_6 \cdot H_2O$.

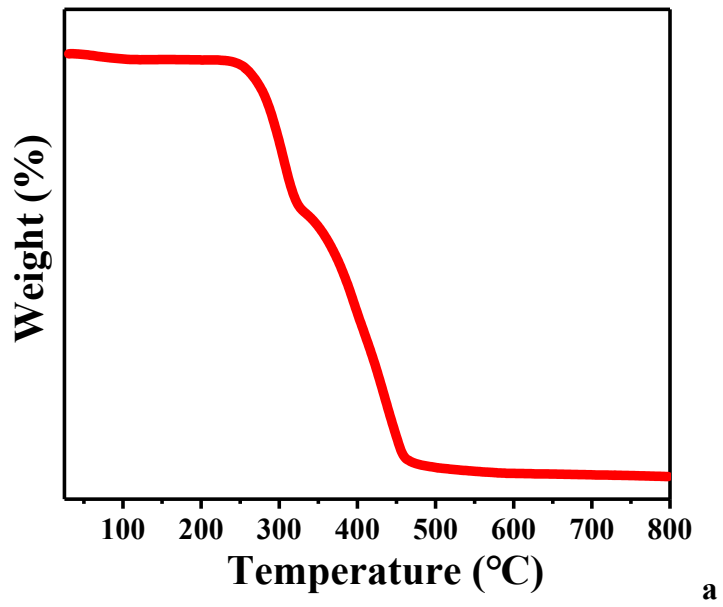

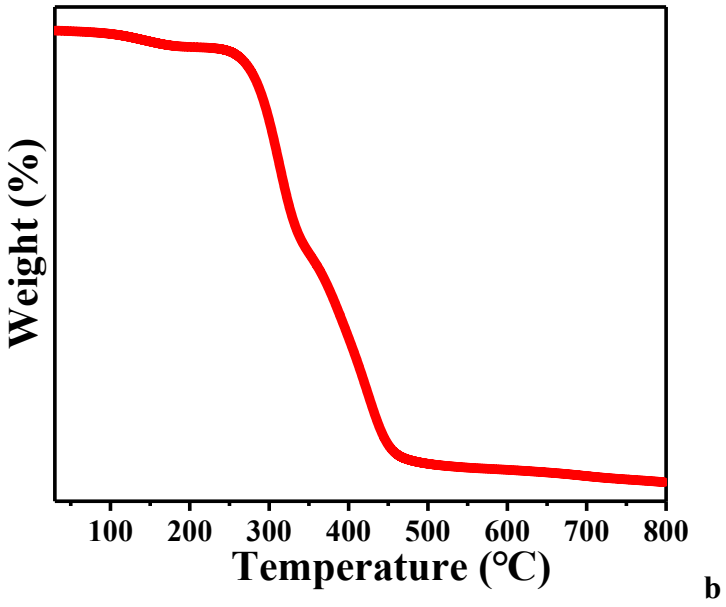

Fig. S17 The thermogravimetric analysis curves of a) (Im-BDMPA)$InCl_6 \cdot H_2O$ and b) (Im-BDMPA)$In_{0.78}Sb_{0.22}Cl_6 \cdot H_2O$.

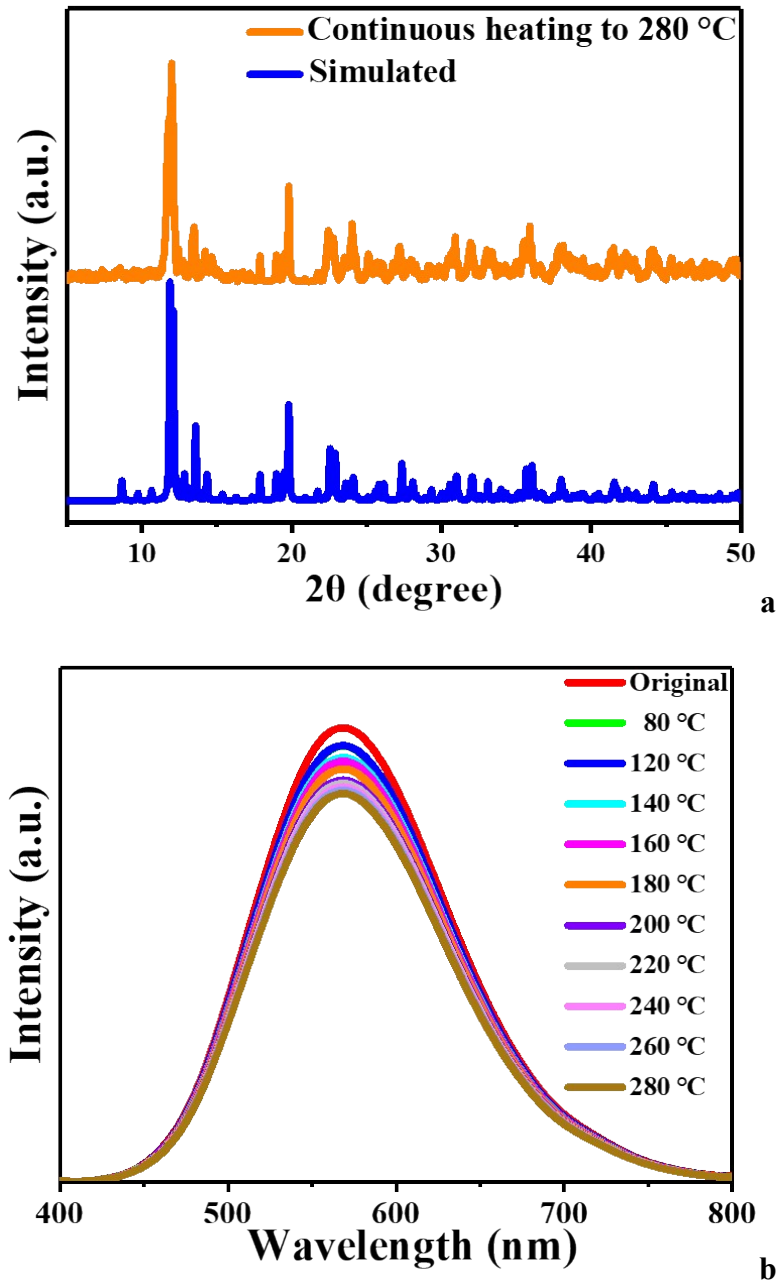

Fig. S18 a) PXRD patterns and b) PL emission spectra of (Im-BDMPA)$In_{0.78}Sb_{0.22}Cl_6 \cdot H_2O$ after continuous heating at different temperature.

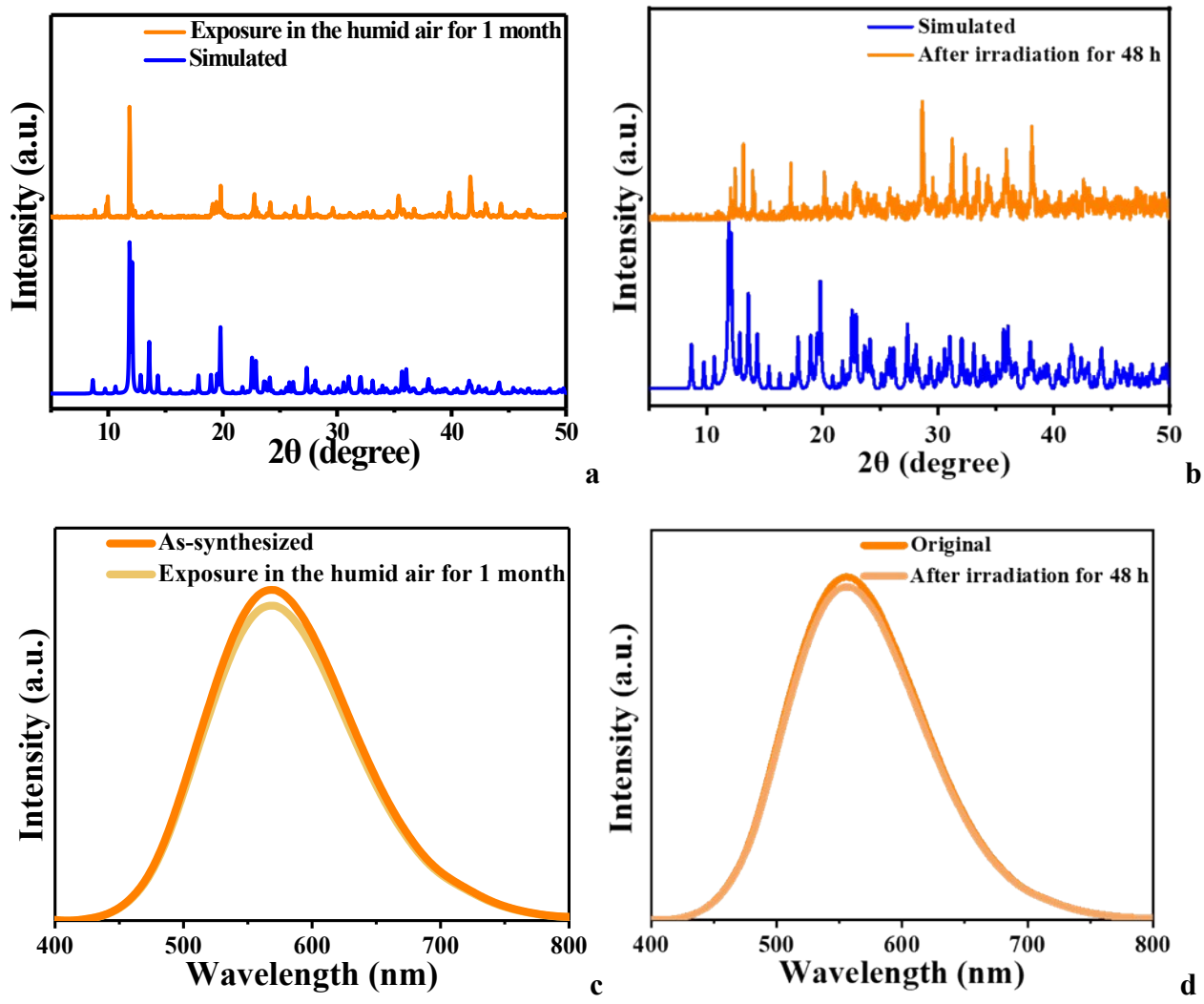

Fig. S19 a-b) The experimental PXRD patterns and c-b) PL emission spectra of (Im-BDMPA)$In_{0.78}Sb_{0.22}Cl_6 \cdot H_2O$ after exposure in humid air for one month or under irradiation of strong UV light for 48 h.

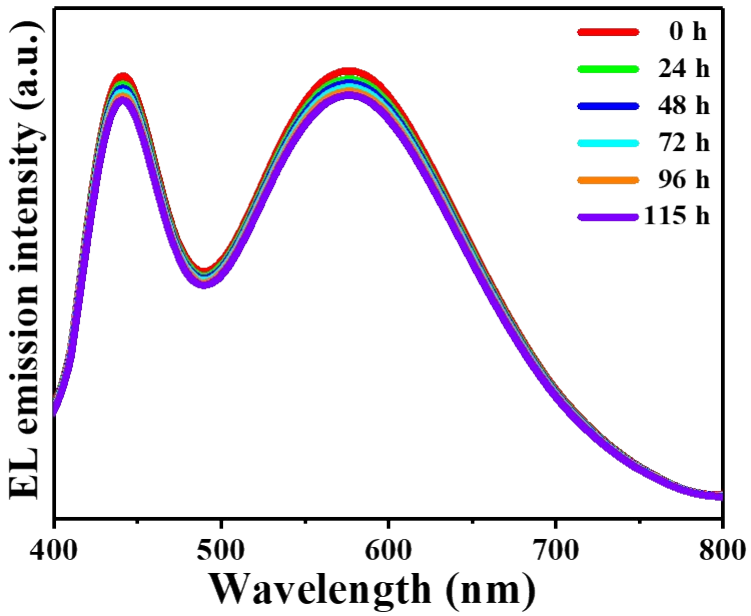

Fig. S20 Time dependent EL emission spectra of fabricated white LED.

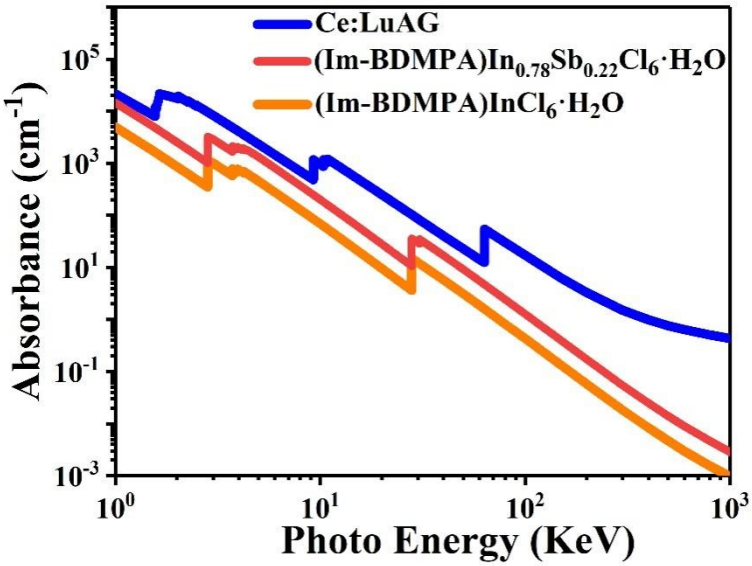

Fig. S21 Absorption coefficients as a function of photon energy from 1 KeV to 1000 KeV of (Im-BDMPA)$In_{1-x}Sb_xCl_6 \cdot H_2O$ and Ce:LuAG.

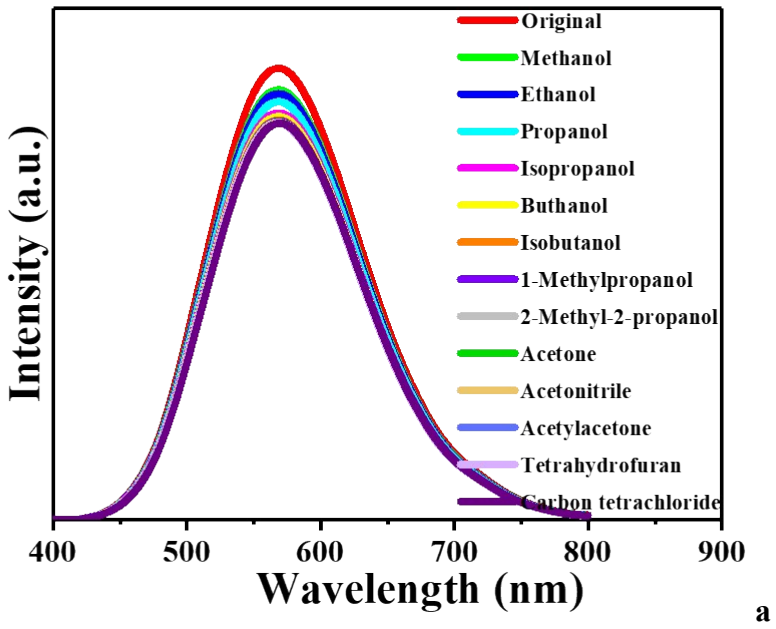

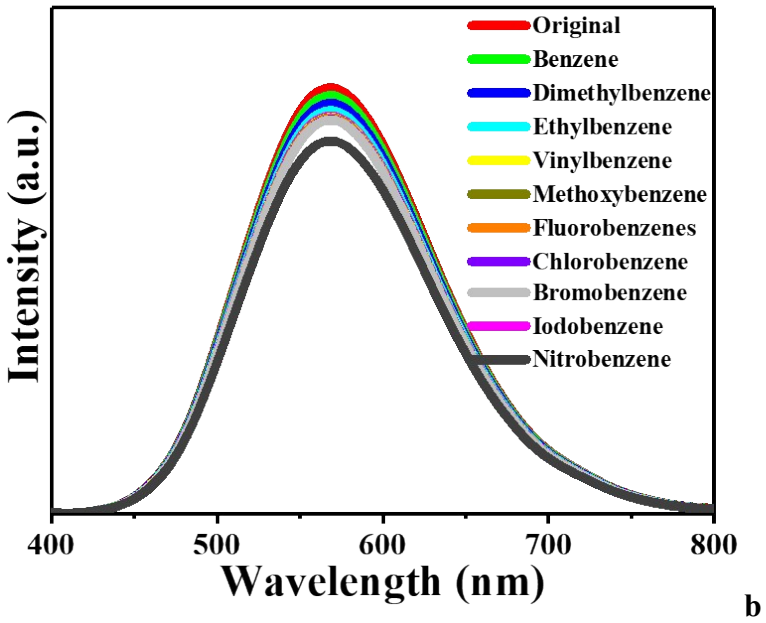

Fig. S22 The PL emission spectra of (Im-BDMPA)$In_{0.78}Sb_{0.22}Cl_6 \cdot H_2O$ based thin film after soaking in various organic solvents.

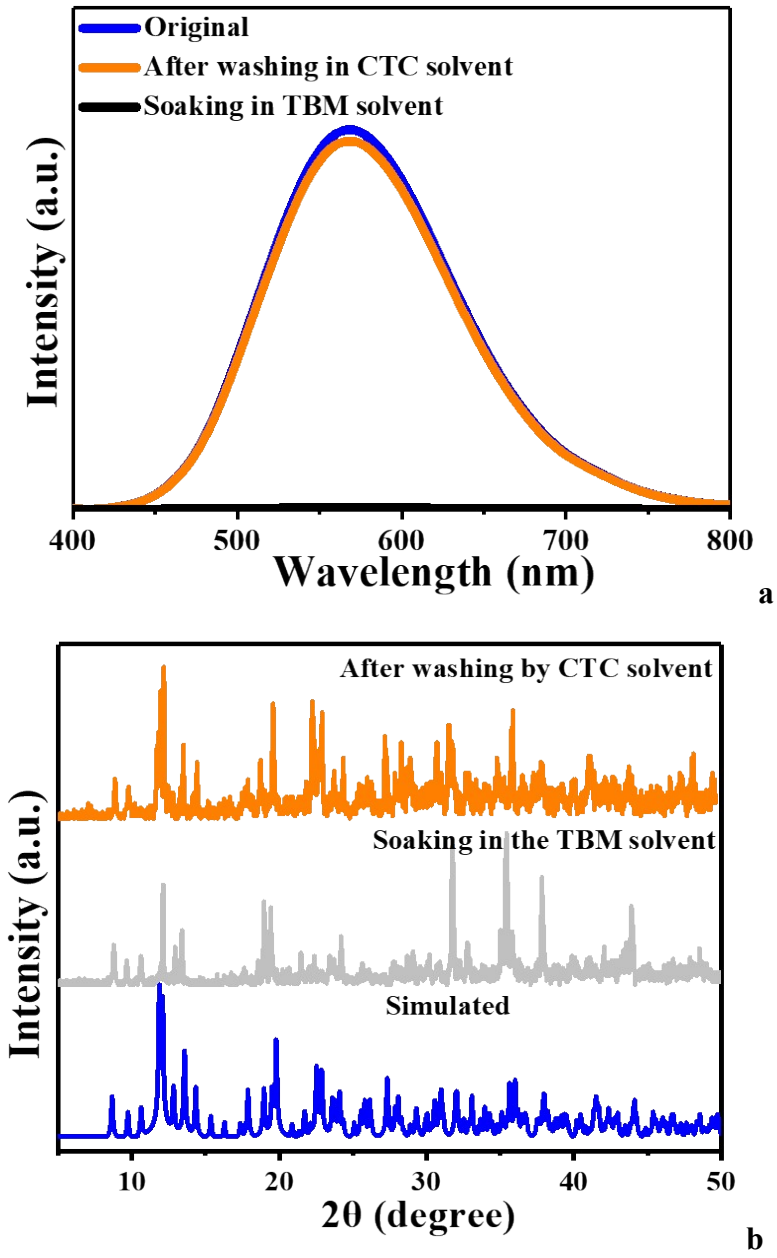

Fig. S23 a) Comparisons of PL emision spectra and b) PXRD patterns of (Im-BDMPA)$In_{0.78}Sb_{0.22}Cl_6 \cdot H_2O$-based film after soaking-drying cycle in tribromethane (TBM) and carbon tetrachloride (CTC) with as-synthesized bulk crystal.

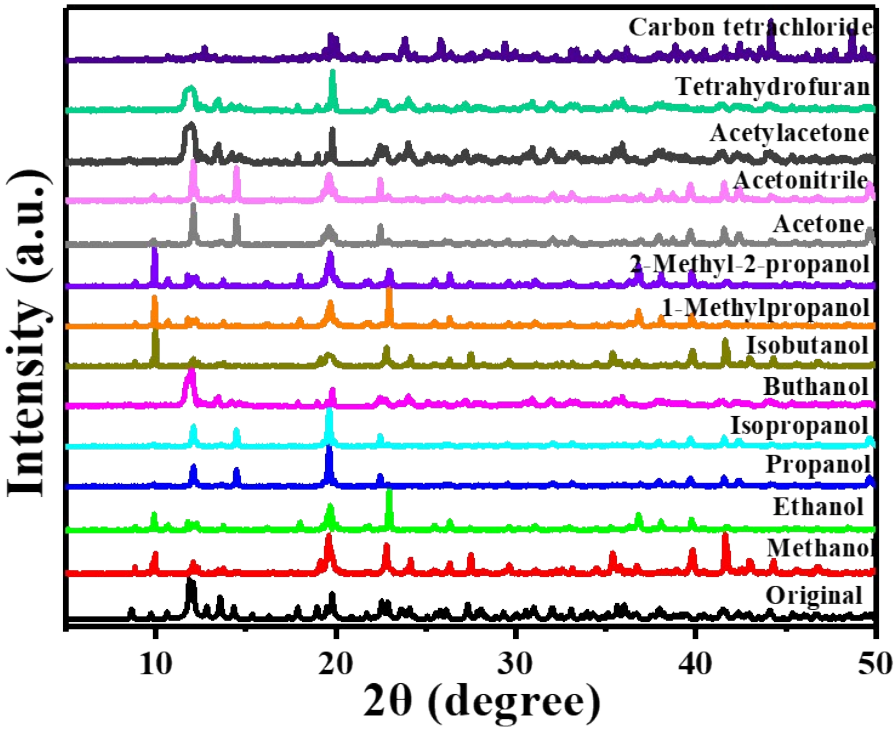

Fig. S24 PXRD patterns of (Im-BDMPA)$In_{0.78}Sb_{0.22}Cl_6 \cdot H_2O$-based thin film after soaking in various organic solvents.

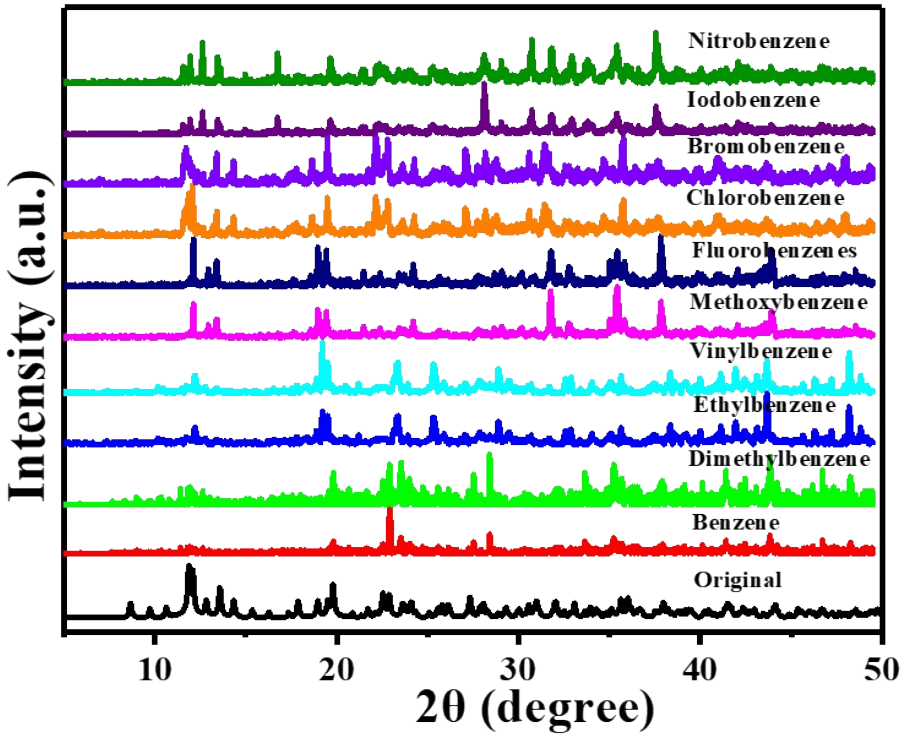

Fig. S25 PXRD patterns of (Im-BDMPA)$In_{0.78}Sb_{0.22}Cl_6 \cdot H_2O$-based thin film after soaking in various organic solvents.

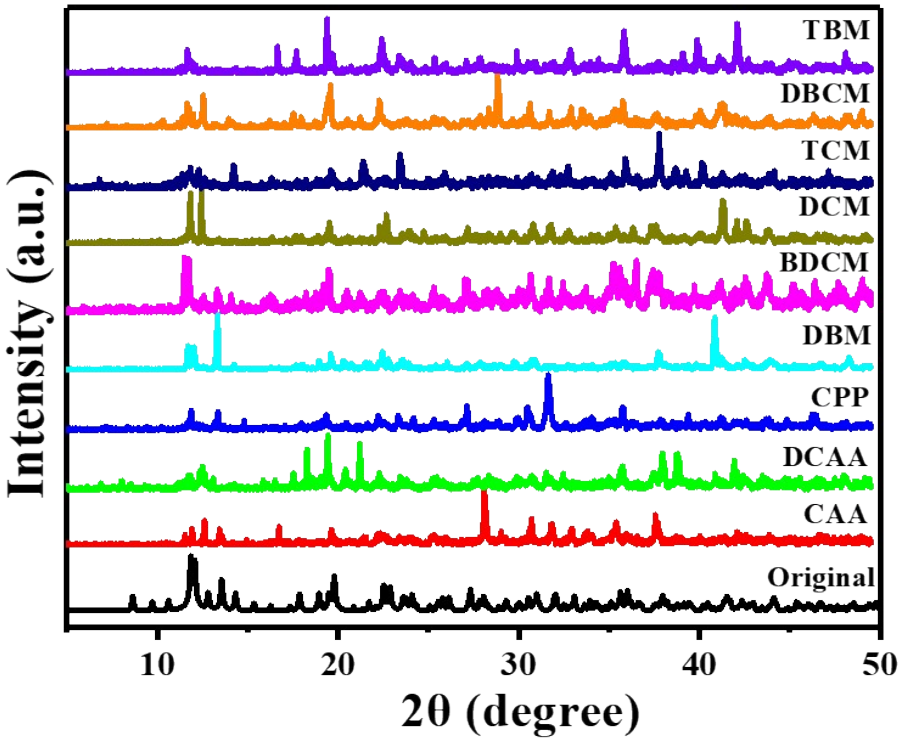

Fig. S26 PXRD patterns of (Im-BDMPA)$In_{0.78}Sb_{0.22}Cl_6 \cdot H_2O$-based thin film after soaking in various organic solvents of chloroacetic acid (CAA), dichloroacetic acid (DCAA), chloropropiophenone (CPP), dibromomethane (DBM), bromodichloromethane (BDCM), dichloromethane (DCM), trichloromethane (TCM), dibromo-monochloro-methane (DBCM), tribromomethane (TBM).

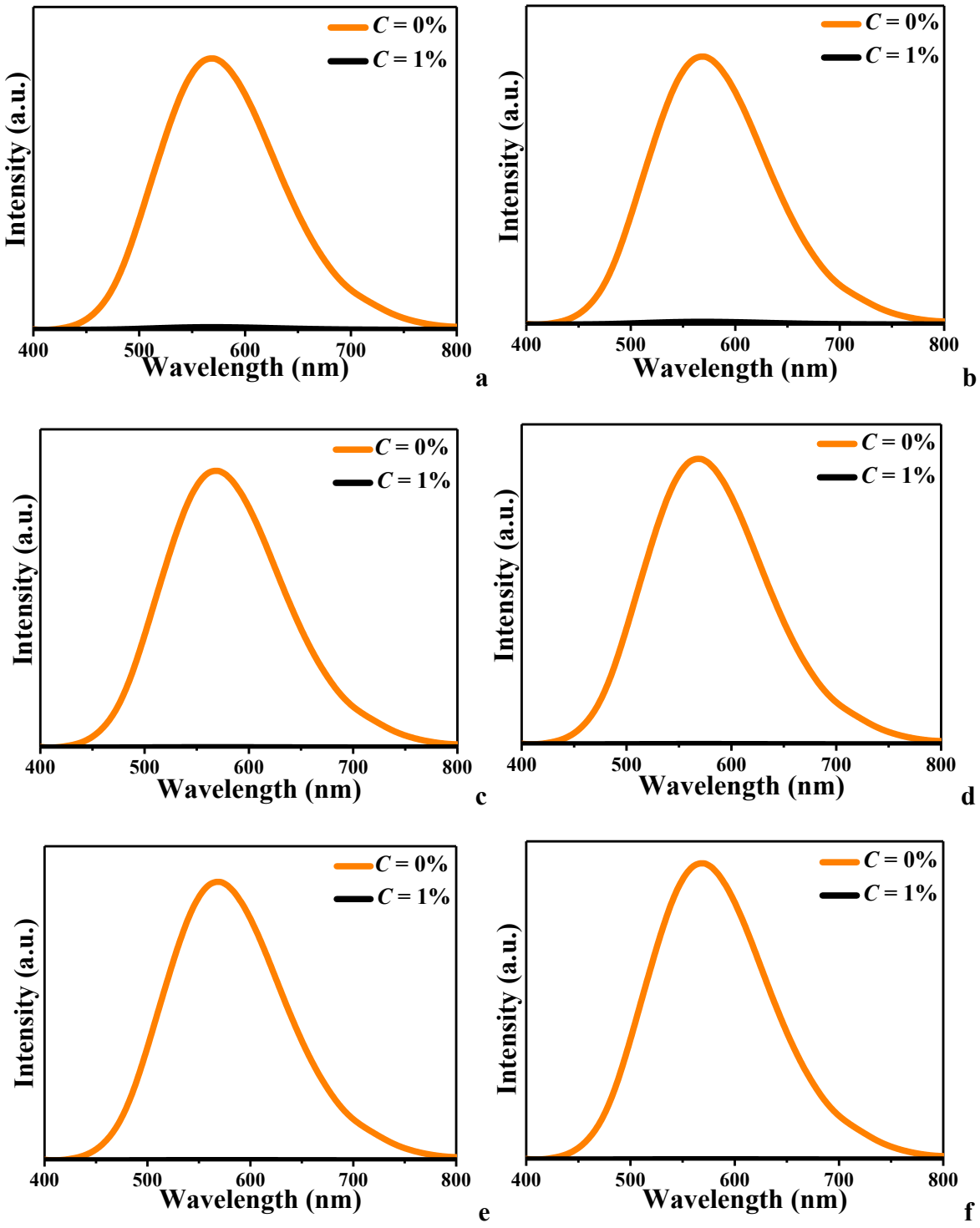
C = 0%
C = 1%
Intensity (a.u.)
400
500
600
700
800
Wavelength (nm)
a
b
c
d
e
f

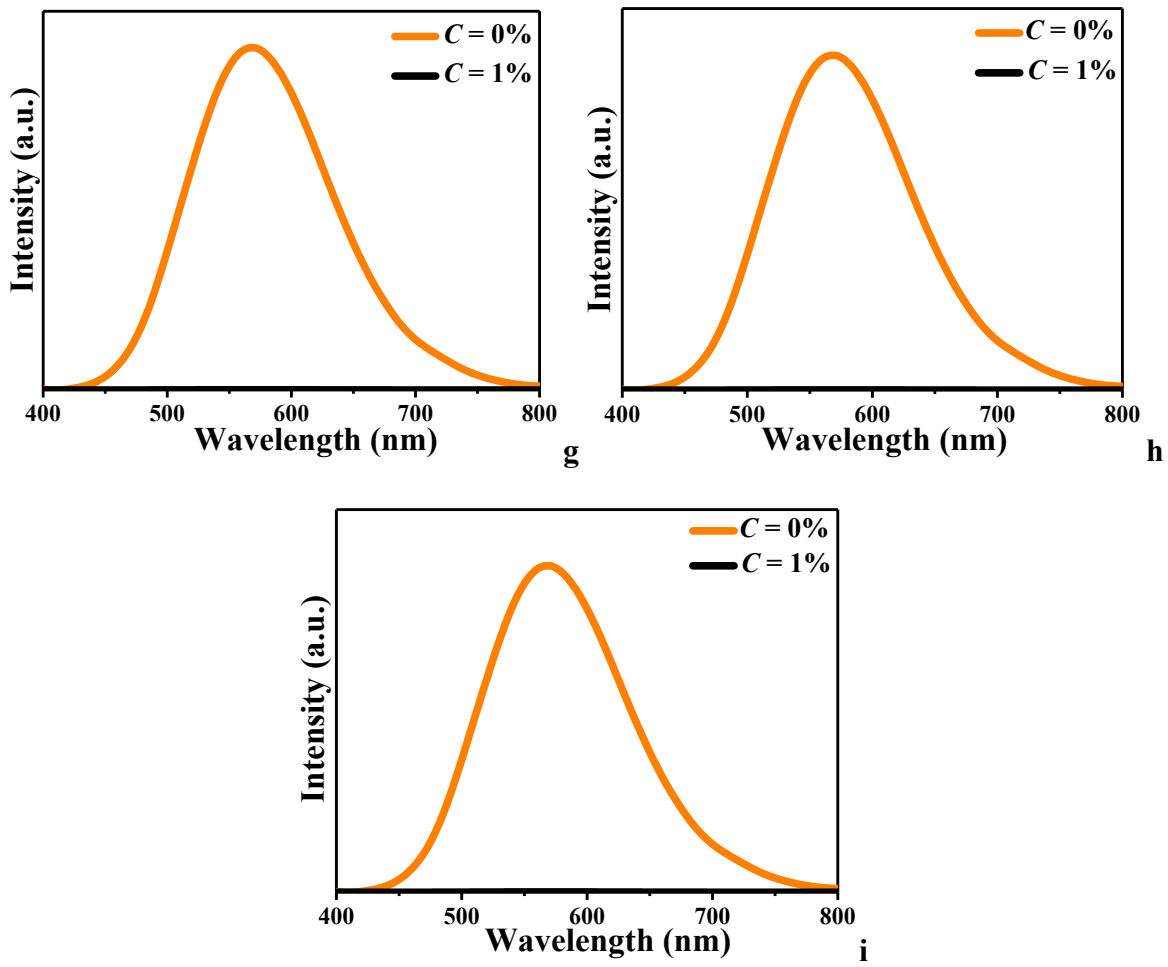

Fig. S27 Comparison of PL emission spectra of (Im-BDMPA)$In_{0.78}Sb_{0.22}Cl_6 \cdot H_2O$-based film toward TBM in various organic solvents including CAA (a), DCAA (b), CPP (c), DBM (d), BDCM (e), DCM (f), TCM (g), DBCM (h) and CTC (i) with concentrations of 0% and 1%.

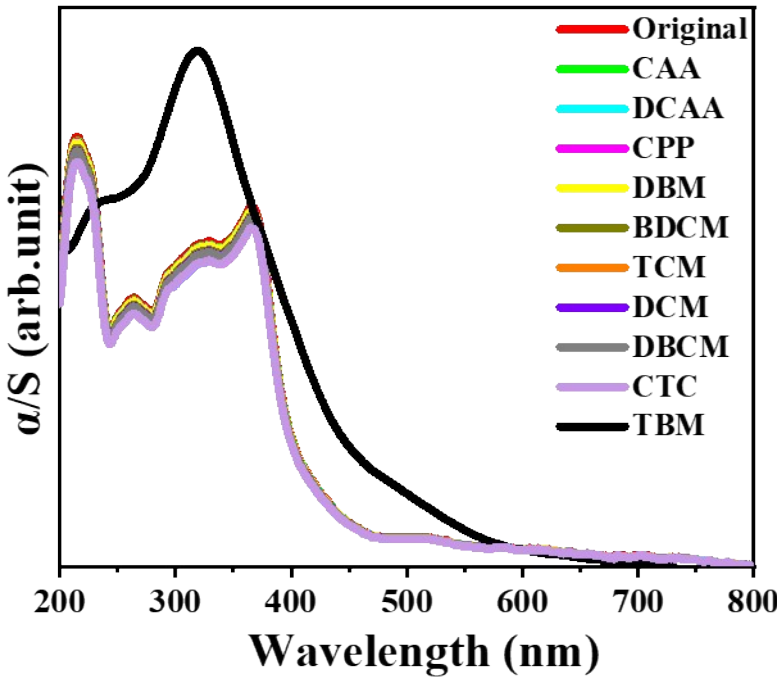

Fig. S28 UV-vis absorption spectra of (Im-BDMPA)$In_{0.78}Sb_{0.22}Cl_6 \cdot H_2O$ microcrystals after soaking in various organic solvents including chloroacetic acid (CAA), dichloroacetic acid (DCAA), chloropropiophenone (CPP), dibromomethane (DBM), bromodichloromethane (BDCM), dichloromethane (DCM), trichloromethane (TCM), dibromo-monochloro-methane (DBCM), tribromomethane (TBM).

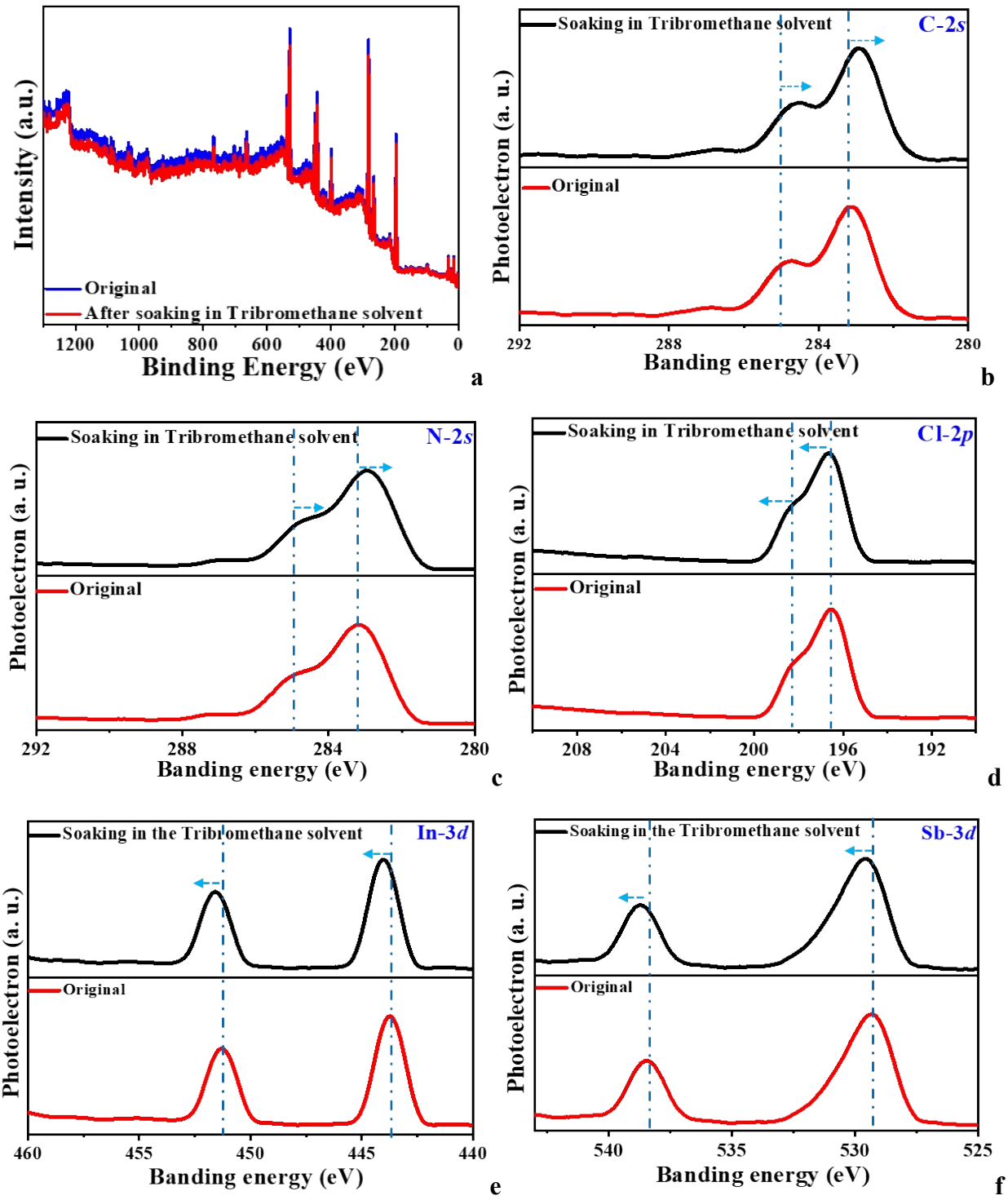

Fig. S29 XPS spectra of (Im-BDMPA)$In_{0.78}Sb_{0.22}Cl_6 \cdot H_2O$ before and after soaking in tribromomethane.

Table S1. Summary of the PL properties of single crystalline indium perovskites.

Material	Emission (nm)	PLQY (%)	FWHM (nm)	Lifetime (μs)	Ref.
(Im-BDMPA)$In_{0.78}Sb_{0.22}Cl_6 \cdot H_2O$	**570**	**95.8**	**135**	**7.85**	**This work**
$Sb@Cs_2InCl_5$	550	95.5	---	---	*Adv. Opt. Mater.* **2021**, *13*, 2002267.
$[MP]_2In_{0.73}Sb_{0.27}Cl_7 \cdot 6H_2O$	525	93.34	107	6.746	*Angew. Chem. Int. Ed.* **2022**, *61*, e202206437
$Sb@Cs_2KInCl_6$	495	93	--	0.26	*Chem. Mater.* **2020**, *32*, 5118-5124.
$Sb@[DAPEDA]InCl_6 \cdot Cl \cdot H_2O$	530	89.29	114	4.94	*CCS. Chem.* **2021**, *3*, 3341-3356.
$Sb@[DPA]_3InCl_6$	520	85.84	113	4.45	*CCS. Chem.* **2021**, *3*, 3341-3356.
$Sb@Cs_2InCl_5 \cdot H_2O$	610	73	164	4.2	*CCS. Chem.* **2020**, *2*, 216-224.
$Sb@Cs_2InBr_5 \cdot H_2O$	692	54.2	207	--	*CCS. Chem.* **2020**, *2*, 216-224.
$[MP]_2InCl_7 \cdot 6H_2O$	512	49.06	111	2.28	*Angew. Chem. Int. Ed.* **2022**, *61*, e202206437
(Im-BDMPA)$InCl_6 \cdot H_2O$	**561**	**48.46**	**134**	**6.35**	**This work**
$[DAPEDA]InCl_6 \cdot Cl \cdot H_2O$	520	40.40	116	3.31	*CCS. Chem.* **2021**, *3*, 3341-3356.
$(PMA)_3InBr_6$	610	35	132	1.26	*Inorg. Chem.* **2019**, *22*, 15602-15609.
$[DPA]_3InCl_6$	510	34.01	108	3.18	*CCS. Chem.* **2021**, *3*, 3341-3356.
$Cs_2InBr_5 \cdot H_2O$	695	33	--	1.65	*Angew. Chem. Int. Ed.* **2019**, *58*, 5277-5281.

PMA = $C_6H_5CH_2NH_3$; DAPEDA = $C_8H_{22}N_4$; DPA = $C_6H_{15}N$.

Table S2. Summary of CIE chromaticity coordinates, CCT and CRI of mixed (Im-BDMPA)$In_{1-x}Sb_xCl_6 \cdot H_2O$ and $BaMgAl_{10}O_{17}:Eu^{2+}$ with different radios.

	CIE chromaticity coordinates	CCT (K)	CRI
1	(0.29,0.25)	9520	95.4
2	(0.31,0.30)	9110	94.2
3	(0.32,0.30)	8990	94.7
4	(0.33,0.33)	6200	96.4
5	(0.34,0.34)	5500	95.4
6	(0.34,0.35)	4120	94.2
7	(0.36,0.36)	3700	95.1
8	(0.38,0.36)	3320	94.5

Table S3. Summary of CIE chromaticity coordinates, CCT and CRI of white LED under different current.

Current (mA)	CIE chromaticity coordinates	CCT (K)	CRI
20	(0.33,0.34)	4250	93.1
40	(0.34,0.33)	4370	92.5
60	(0.33,0.33)	4420	94.3
80	(0.34,0.34)	4470	93.6
100	(0.35,0.34)	4530	94.4
120	(0.35,0.33)	4590	95.4

Table S4. Summary of X-ray scintillation performance of 0D hybrid metal halides.

Materials	Grow method	Maximum emission (nm)	Light yield (photons/ MeV)	Detection limit (μGy/s)	Ref.
(Im-BDMPA)$In_{0.78}Sb_{0.22}Cl_6 \cdot H_2O$	**Solution method**	**569**	**55320**	**0.0853**	**This work**
CsI(TI)	Non-vacuum crucible descent	550	54000	---	1
$Cs_3Cu_2I_5$: single crystal	Bridgman method	500	51000	---	2
$(PPN)_2SbCl_5$	Antisolvent diffusion	635	49000	0.194	3
CsI(Na)	Non-vacuum crucible descent	420	41000	---	4
β-$Cs_3Cu_2Cl_5$	Hot-injection	525	34000	0.1746	5
LYSO	Medium frequency induction heating	410	33000	---	6
$Cs_3Cu_2I_5$ single crystal	Bridgman method	440	32000	---	7
$CdWO_4$	Pulling method	480	28000	---	8
K_2CuBr_3 single crystal	Cooling method	391	23806	132.8	9
Ce:LuAG	Float-zone method	500	25000	---	10
(Im-BDMPA)$InCl_6 \cdot H_2O$	**Solution method**	**570**	**23047**	**---**	**This work**
$CsPbBr_3$ QDs	Single-step injection	520	21000	---	10
Rb_2CuCl_3	Cooling method	4001	16600	88.5	11

Table S5. Crystal Data and Structural Refinements for (Im-BDMPA)$InCl_6 \cdot H_2O$.

Compound	(Im-BDMPA)$InCl_6 \cdot H_2O$
chemical formula	$C_{10}H_{28}N_3OInCl_6$
Fw	533.887
Space group	$P2_12_12_1$
a/Å	9.3561(1)
b/Å	12.3477(2)
c/Å	18.1889(3)
α/°	90
β/°	90
γ/°	90
V(Å^3)	2101.30(5)
Z	4
D_{calcd} (g·cm^{-3})	1.688
Temp (*K*)	296.15
μ (mm^{-1})	1.899
F(000)	1073
Reflections collected	26504
Unique reflections	6525
GOF on F^2	1.017
R_1,wR_2($I>2\sigma(I)$)[a]	0.0237, 0.0543
R_1,wR_2(all data)	0.0276, 0.0558

[a] $R_1 = \sum||F_o| - |F_c||/\sum|F_o|$, $wR_2 = \{\sum w[(F_o)^2 - (F_c)^2]^2/\sum w[(F_o)^2]^2\}^{1/2}$

Table S6. Selected bond lengths (Å) and bond angles (°) for (Im-BDMPA)$InCl_6 \cdot H_2O$.

In1-Cl1	2.5009(6)	Cl1-In1-Cl6	91.68(2)
In1-Cl2	2.5452(6)	Cl2-In1-Cl3	87.73(2)
In1-Cl2[1]	2.5269(6)	Cl2-In1-Cl5	93.50(2)
In1-Cl3	2.5231(6)	Cl2-In1-Cl6	175.15(2)
In1-Cl3[1]	2.5026(6)	Cl3-In1-Cl5	175.80(2)
In1-Cl4	2.5363(6)	Cl3-In1-Cl6	88.55(2)
		Cl4-In1-Cl2	89.88(2)
Cl1-In1-Cl2	85.39(2)	Cl4-In1-Cl3	88.89(2)
Cl1-In1-Cl3	92.76(2)	Cl4-In1-Cl5	87.10(2)
Cl1-In1-Cl4	174.93(2)	Cl4-In1-Cl6	93.16(2)
Cl2-In1-Cl5	91.34(2)	Cl6-In1-Cl5	90.43(2)

Table S7. Hydrogen bonds data for (Im-BDMPA)$InCl_6 \cdot H_2O$.

D-H···A	d(D-H)	d(H···A)	d(D···A)	<(DHA)
N2-H13···Cl3	0.900(3)	2.828(2)	3.372(2)	120.2(2)
N2-H13···Cl6	0.900(3)	2.828(2)	3.302(2)	154.6(2)
N2-H14···Cl2	0.900(3)	2.730(2)	3.328(2)	124.93(19)
N2-H14···Cl3	0.900(3)	2.662(2)	3.492(2)	153.7(2)
O1-H27···N3	0.85(3)	2.05(3)	2.888(3)	168(3)
O1-H29···Cl4	0.85(3)	2.45(4)	3.276(3)	164(3)
C2-H4···Cl2	0.960(9)	2.605(11)	3.551(3)	169.1(13)
C4-H29···Cl5	0.970(3)	2.714(3)	3.566(3)	146.9(2)
C3-H10···Cl3	0.970(4)	2.714(3)	3.568(3)	147.2(3)
C9-H10···Cl5	0.970(4)	2.714(4)	3.568(3)	147.2(3)

Reference

[1] J. J. Ma, W. J. Zhu, L. Lei, D. G. Deng, Y. J. Hua, Y. M. Yang, S. Q. Xu, P. N. Prasad, *ACS Appl. Mater. Interfaces*. 2021, **13**, 44596-44603.

[2] D. Yuan, *ACS Appl. Mater. Interfaces.* 2022, **12**, 38333-38340.

[3] Q. He, C. Zhou, L. Xu, S. Lee, X. Lin, J. Neu, M. Worku, M. Chaaban, B. W. Ma, *ACS Mater. Lett.* 2020, **2**, 633-638.

[4] G. F. Carpenter, M. J. Coe, A. R. Engel, *Nature*. 1976, **99**, 259.

[5] Q. Zhou, J. W. Ren, J. W. Xiao, L. Lei, F. Y. Liao, H. P. Di, C. Wang, L. J. Yang, Q. Chen, X. F. Yang, Y. Y. Zhao, X. D. Han, *Nanoscale.* 2021*,* **13**, 19894.

[6] R. J. Sun, Z. F. Wang, H. Q. Wang, Z. H. Chen, Y. G. Yao, H. P. Zhang, Y. N. Gao, X. T. Hao, H. Q. Liu, Y. H. Zhang, *ACS Appl. Mater. Interfaces*. 2022, **14**, 36801-36806.

[7] S. Cheng, A. Beitlerova, R. Kucerkova, M. Nikl, G. Ren, Y. Wu, *Phys. Status Solidi RRL*. 2020, **14**, 2000374.

[8] A. G. Gandhi, H. H. Chiu, M. K. Ho, T. E. Hsu, T. Y. Li, Y. H. Wu, B. V. Kumar, P. M. Reddy, B. H. Lin, C. L. Cheng, S. Y. Wu, *ACS Appl. Nano Mater.* 2022, **5**, 14811-14823.

[9] W. Gao, G. Niu, L. Yin, B. Yang, J. H. Yuan, D. Zhang, K. H. Xue, X. Miao, Q. Hu, X. Du, *ACS Appl. Electron. Mater.* 2020, **2**, 2242-2249.

[10] Y. H. Zhang, R. J. Sun, X. Y. Ou, K. F. Fu, Q. S. Chen, Y. C. Ding, L. J. Xu, L. M. Liu, Y. Han, A. V. Malko, X. G. Liu, H. G. Yang, O. M. Bakr, H. Liu, O. F. Mohammed, *ACS Nano*. 2019, **13**, 2520-2525.

[11] X. Zhao, G. Niu, J. Zhu, B. Yang, J. H. Yuan, S. Li, W. Gao, Q. Hu, L. Yin, K. H. Xue, *J. Phys. Chem. Lett.* 2020, **11**, 1873-1880.